parametric maps (SPM) were computed from local MR signals using a linear multiple regression with conditions (modelled as two temporal basis functions) and runs as co-variates[26]. Only regions formed by more than 12 contiguious active voxels ($P < 0.05$) were analysed. The main effect of dual-task (and delayed-response, respectively) performance was computed by selecting the regions which were co-jointly significantly activated in the dual-task (delay) and branching conditions compared with the control and delay (dual-task) conditions ($Z > 5.4$, $P < 0.0005$, corrected for multiple comparisons). The additive effect of delay and dual-task performance was observed in the regions co-jointly and significantly activated in all conditions compared with the baseline ($Z > 5.4$, $P < 0.0005$, corrected). No interaction between those factors ($P > 0.05$, uncorrected) was observed in those regions. Branching-specific activations were computed as the regions with significant activations in the branching condition compared with the control ($Z > 5.4$, $P < 0.0005$, corrected) and with a significant interaction between the delayed-response and dual-task factors (branching and control compared to delay and dual-task conditions; $P < 0.0005$, uncorrected). The same branching-specific activation was found *post hoc* by computing the voxels co-jointly activated in the branching condition compared separately with all other conditions (fronto-polar: $Z > 5.4$, $P < 0.0005$, corrected; elsewhere $P > 0.05$, corrected). Branching-specific activations were confirmed in five single-subject analyses. They were located bilaterally in the superior fronto-polar gyrus at the crossing of the middle frontal gyrus (two subjects) or in the middle fronto-polar gyrus (three subjects)[28]. Moreover, bilateral fronto-polar activations were replicated in six additional normal right-handed subjects performing the branching and two additional control tasks.

Received 23 October 1998; accepted 12 March 1999.

1. Grafman, J. in *Structure and Function of the Human Prefrontal Cortex* (eds Grafman, J., Holyoak, K. J. & Boller, F.) 337–368 (Annals of the New York Academy of Sciences, New York, 1995).
2. Baker, S. C. *et al.* Neural system engaged by planning: A PET study of the Tower of London task. *Neuropsychologia* **34,** 515–526 (1996).
3. Owen, A. M., Doyon, J., Petrides, M. & Evans, A. C. Planning and spatial working memory: a positron emission tomography study in human. *Eur. J. Neurosci.* **8,** 353–564 (1996).
4. Sirigu, A. *et al.* Planning and script analysis following prefrontal lobe lesions. *Ann. NY Acad. Sci.* **769,** 277–288 (1995).
5. Spector, L. & Grafman, J. in *Handbook of Neuropsychology* (eds Boller, F. & Grafman, J.) 377–392 (Elsevier, Amsterdam, 1994).
6. Wharton, C. & Grafman, J. Reasoning and the human brain. *Trends Cogn. Sci.* **2,** 54–59 (1998).
7. Stuss, D. T. & Benson, D. F. *The Frontal Lobes* (Raven, New York, 1986).
8. Fuster, J. M. *The Prefrontal Cortex. Anatomy, Physiology, and Neuropsychology of the Frontal Lobe* (Raven, New York, 1989).
9. D'Esposito, M. *et al.* The neural basis of the central executive system of working memory. *Nature* **378,** 279–281 (1995).
10. Corbetta, M. Frontoparietal cortical networks for directing attention and the eye to visual locations: identical, independent, or overlapping neural systems? *Proc. Natl Acad. Sci. USA* **95,** 831–838 (1998).
11. Squire, L. R. *et al.* Activation of the hippocampus in normal humans: a functional anatomical study of memory. *Proc. Natl Acad. Sci. USA* **89,** 1837–1841 (1992).
12. Buckner, R. L. *et al.* Functional anatomical studies of explicit and implicit memory retrieval tasks. *J. Neurosci.* **15,** 12–29 (1995).
13. Shallice, T. *et al.* Brain regions associated with acquisition and retrieval of verbal episodic memory. *Nature* **368,** 633–635 (1994).
14. Grady, C. L. *et al.* Age-related reductions in human recognition memory due to impaired encoding. *Science* **269,** 218–221 (1995).
15. Tulving, E. *et al.* Neuroanatomical correlates of retrieval in episodic memory: auditory sentence recognition. *Proc. Natl Acad. Sci. USA* **91,** 2012–2015 (1994).
16. Tulving, E. *Elements of Episodic Memory* (Oxford Science, Oxford, 1983).
17. Galaburda, A. M., LeMay, M., Kemper, T. L. & Geschwind, N. Right-left asymmetrics in the brain. *Science* **199,** 852–856 (1978).
18. Furey, M. L. *et al.* Cholinergic stimulation alters performance and task-specific regional cerebral blood flow during working memory. *Proc. Natl Acad. Sci. USA* **94,** 6512–6516 (1997).
19. Goldman-Rakic, P. C. in *Handbook of Physiology, The Nervous System* (eds Plum, F. & Mountcastle, V.) 373–417 (American Physiological Society, Bethesda, MD, 1987).
20. Petrides, M. in *Handbook of Neuropsychology* (eds Boller, F. & Grafman, J.) 59–82 (Elsevier, Amsterdam, 1994).
21. Jonides, J. *et al.* Spatial working memory in humans as revealed by PET. *Nature* **363,** 623–625 (1993).
22. Courtney, S. M., Ungerleider, L. G., Keil, K. & Haxby, J. V. Transient and sustained activity in a distributed neural system for human working memory. *Nature* **386,** 608–611 (1997).
23. MacLeod, A. K., Buckner, R. L., Miezin, F. M., Petersen, S. E. & Raichle, M.. E. Right anterior prefrontal cortex activation during semantic monitoring and working memory. *NeuroImage* **7,** 41–48 (1998).
24. Grafton, S. T., Hazeltine, E. & Ivry, R. Functional mapping of sequence learning in normal humans. *J. Cogn. Neurosci.* **7,** 497–510 (1995).
25. Pallier, C., Dupoux, E. & Jeannin, X. EXPE: an expandable programing language for on-line psychological experiments. *Behav. Res. Methods Instrum. Comput.* **29,** 322–327 (1997).
26. Friston, K. J., Frith, C. D., Liddle, P. F. & Frackowiak, R. S. J. Comparing functional (PET) images: The assessment of significant change. *J. Cereb. Blood Flow Metab.* **11,** 690–699 (1991).
27. Talairach, J. & Tournoux, P. *Co-planar Stereotaxic Atlas of the Human Brain* (Thieme Medical, New York, 1988).
28. Duvernoy, H. *The Human Brain. Surface, Three Dimensional Sectional Anatomy and MRI.* (Springer, Wien, 1991).

Correspondence and requests for materials should be addressed to J.G. (e-mail: jgr@box-j.nih.gov).

Synaptic calcium transients in single spines indicate that NMDA receptors are not saturated

Zachary F. Mainen, Roberto Malinow & Karel Svoboda

Cold Spring Harbor Laboratory, 1 Bungtown Road, Cold Spring Harbor, New York 11724, USA

At excitatory synapses in the central nervous system, the number of glutamate molecules released from a vesicle is much larger than the number of postsynaptic receptors. But does release of a single vesicle normally saturate these receptors? Answering this question is critical to understanding how the amplitude and variability of synaptic transmission are set and regulated. Here we describe the use of two-photon microscopy[1] to image transient increases in Ca^{2+} concentration mediated by NMDA (*N*-methyl-D-aspartate) receptors in single dendritic spines of CA1 pyramidal neurons in hippocampal slices. To test for NMDA-receptor saturation, we compared responses to stimulation with single and double pulses. We find that a single release event does not saturate spine NMDA receptors; a second release occurring 10 ms later produces ~80% more NMDA-receptor activation. The amplitude of spine NMDA-receptor-mediated [Ca^{2+}] transients (and the synaptic plasticity which depends on this) may thus be sensitive to the number of quanta released by a burst of action potentials and to changes in the concentration profile of glutamate in the synaptic cleft.

The issue of receptor saturation has been controversial, partly owing to complexities in the interpretation of indirect experiments[2]. A direct test for saturation is to examine the interaction between two synaptic currents occurring in rapid sequence[3,4]. Receptor saturation during the first event will block the response to a second event that occurs before transmitter has had a chance to unbind from the receptors. Glutamate unbinding from NMDA receptors occurs slowly ($\tau > 100$ ms)[5,6]. Although it is conceptually simple, this experiment is complicated by the probabilistic nature of transmitter release. Because only a fraction of stimulated synapses release transmitter, the first and second responses might not occur at the same synapses, as is required for the interaction test. A reliable way to detect failure and release of transmitter at a single synapse is therefore required.

We used two-photon-laser scanning microscopy (2PLSM)[1] to monitor synaptic activation by measuring [Ca^{2+}] transients in postsynaptic spines[7]. Dendritic spines on CA1 pyramidal cells have a single postsynaptic density[8] associated with a single apposing presynaptic active zone[9]. Ca^{2+} entering spines through NMDA-receptor (NMDA-R) channels is therefore a direct reflection of NMDA-R activation at single synapses. We filled neurons in brain slices by whole-cell recording with a high-affinity Ca^{2+} indicator and activated synapses by extracellular stimulation using a glass pipette placed close to an apical dendritic branch[10]. Synaptic [Ca^{2+}] transients were imaged using either frame (16 Hz; Fig. 1) or line-scan (500 Hz; Fig. 2) mode. Frame mode allowed us to discriminate between anatomically distinct Ca^{2+} sources and thereby to isolate [Ca^{2+}] signals arising from single spines (Fig. A in Supplementary Information).

To isolate NMDA-R-mediated Ca^{2+} influx, neurons were voltage-clamped at positive potentials (above synaptic reversal potential; Fig. 2c) to allow opening of NMDA receptors, inactivate voltage-sensitive Ca^{2+} channels (Fig. B in Supplementary Information), and minimize the effects of possible synaptic voltage escape. Under these conditions, fluorescence transients were unaffected by the selective

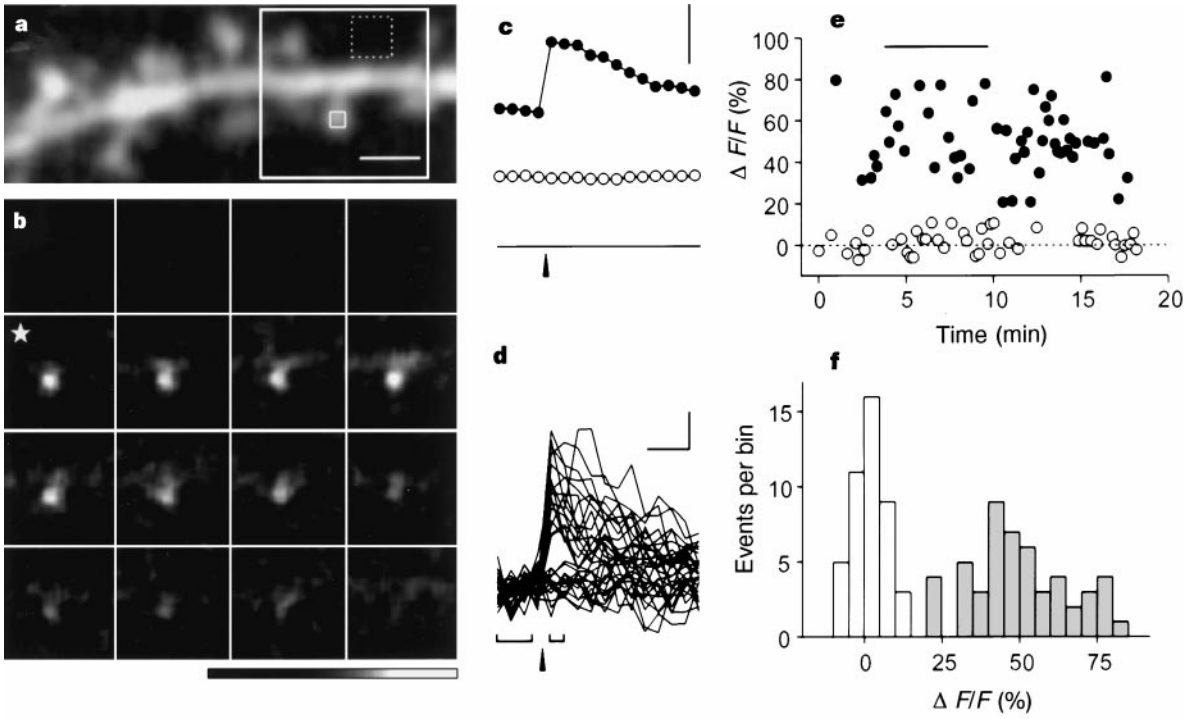

Figure 1 Probabilistic activation of NMDA receptors monitored by imaging spine [Ca^{2+}] transients. **a**, Fluorescence image of tertiary apical dendritic branch of a CA1 pyramidal neuron. Scale bar: 2 μm. **b**, Sequence of frames (64 ms per frame, area shown by large box in **a**) showing relative change in fluorescence ($\Delta F/F(t)$) during synaptic stimulation (asterisk shows stimulus time). Grey scale: –5 to 90% $\Delta F/F$. **c**, Average fluorescence ($F(t)$) measured at spine (small solid box, filled symbols) and background (dashed box, open symbols). Arrowhead indicates stimulation time; thin line indicates 0 level. Scale bar: 20 arbitrary units. **d**, 34 spine responses collected in the period indicated by horizontal bar in **e**. Scale bars: 25% $\Delta F/F$, 200 ms. **e**, Amplitude of fluorescence transients showing failures (open symbols) and releases (filled symbols). **f**, Corresponding histogram of response amplitudes.

AMPA (β-amino-3-hydroxy-5-methyl-4-isoxazole propionic acid) receptor antagonist NBQX (2,3-dihydroxy-6-nitro-7-sulphamoyl-benzo quinoxaline) (5–10 μM) and blocked by the NMDA-R antagonist D-CPP (*R*(−)-3-(2-carboxypiperazine-4-yl)-propyl-1-phosphonic acid) (10 μM; 4.2 ± 3.5% of control, $n = 5$). Fluorescence transients peaked at around 50–100 ms after a stimulus (Fig. 2b), consistent with the time course of the NMDA-R current[5] (Fig. 2c), and decayed slowly (probably mainly reflecting unbinding of Ca^{2+} from the indicator[11]). To test for a possible contribution of Ca^{2+} release from intracellular stores, we inhibited store refilling by using cyclopiazonic acid (CPA). In control experiments (see Methods), CPA treatment (30 μM) increased the decay time of action-potential-evoked dendritic fluorescence transients to 167 ± 11% of control ($n = 3$, $P < 0.002$), showing that the drug was effective[12]. CPA had no effect on the amplitude of synaptic fluorescence transients (93 ± 8% of control ($n = 3$); compared to 95 ± 4% ($n = 5$) over a similar time period in untreated slices), showing that release from stores does not contribute to spine [Ca^{2+}] transients under these conditions.

Synaptically activated spine fluorescence transients mediated by NMDA-Rs were large enough to distinguish successful transmitter release from failure of release (Fig. 1d–f), and could be monitored for up to ~500 trials (stimulation rate, 0.2 Hz). The probability of release measured at different synapses was broadly distributed (mean, 0.38, s.d. = 0.23; $n = 32$). Fluorescence transients showed greater trial-to-trial amplitude variability than the background noise ($s.d._{noise} = 5.1 \pm 0.4\%\ \Delta F/F$, $s.d._{resp} = 15.9 \pm 1\%\ \Delta F/F$, noise-subtracted coefficient of variation (c.v.) = 0.34 ± 0.02, $n = 27$; $\Delta F/F$ is the relative fluorescence). Failure and response distributions were well separated (on average, $2 \times s.d._{noise} < mean_{resp} - 2 \times s.d._{resp}$). Consistent with previous electrophysiological measurements[13,14,16,17], responses showed pronounced paired-pulse facilitation (PPF) that was inversely related to release probability. The probability of at least one release increased to 0.75 ± 0.22 for a pair of stimuli 10 ms apart, implying PPF = 2.08 ± 0.87 (see Methods).

To test for receptor saturation, we compared NMDA-R-spine [Ca^{2+}] transients produced by single stimuli to those produced by pairs of stimuli separated by 10 ms (Figs 2, 3). At this delay, glutamate that bound to NMDA-Rs during the first release will still occupy the receptors, owing to its slow unbinding rate[5,6] (Fig. 2c). If receptors are saturated by a single release of glutamate then there will be no unbound receptors available for opening by a subsequent release. The expected response for a stimulus pair would therefore be about the same as for one stimulus. In fact, the average fluorescence transients evoked by pairs of stimuli were significantly larger than those evoked by single stimuli (Figs 2b, 3a, b) and the distributions of responses to stimulus pairs were shifted to larger amplitudes (Fig. 3c). Quantal peaks were not apparent in the distributions of paired stimulus responses, probably because of the large variance of single quantal NMDA-R responses. Similar shifts in response amplitudes were observed in all synapses examined (Fig. 3d; single stimulus response $r_1 = 43.8 \pm 2.8\%\ \Delta F/F$, paired stimulus response $r_{1+2} = 55.1 \pm 3.2\%\ \Delta F/F$, $n = 27$, $P < 10^{-9}$, paired sign test). Glutamate released following a single action potential therefore does not saturate postsynaptic NMDA-Rs.

What fraction of NMDA-Rs remain available for binding after one release event? Owing to the slow rise time of [Ca^{2+}] transients mediated by NMDA-Rs (Fig. 2b), we could not distinguish between instances of single and double transmitter release in response to pairs of stimuli. Instead, we used a simple model to estimate the

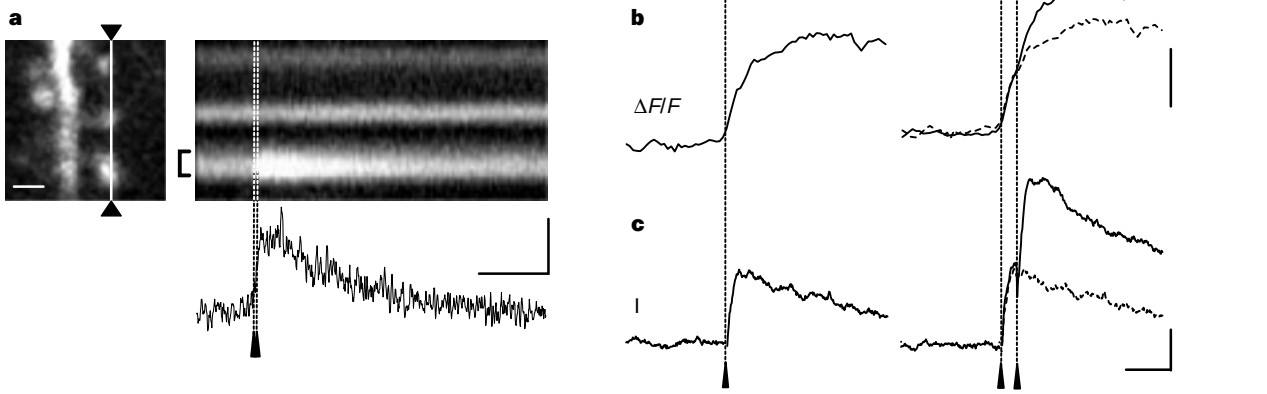

Figure 2 Time course of NMDA-R currents and spine fluorescence transients. Single or pairs of stimuli were delivered on alternating trials. **a** (left), Vertical line indicates the placement of the line scan (scale bar: 1 μm). **a** (right), Line scan in which vertical dimension corresponds to the image (left) and the horizontal dimension represents time. Stimulus times indicated by arrowheads. Below: $\Delta F/F(t)$ at the bottom spine (averaged over window indicated by brackets). Scale bars: 250 ms, 50% $\Delta F/F$. **b**, **c**, Average EPSC (vertical bar, left in **c**) and corresponding $\Delta F/F(t)$ (**b**) for single (left) and double (right) stimuli at the same spine as **a**. The time base in **a** is expanded in **b** and **c**. The EPSC (and hence peak open probability) peaks at ~10 ms (when the second stimulus is delivered). Scale bars: 25% $\Delta F/F$, 100 pA, 25 ms.

number of double releases based on the failure rates for single and paired stimuli (see Methods). We could then obtain a prediction for the ratio of paired to single response amplitudes (r_{1+2}/r_1; both excluding failures), assuming linear summation. We assume a single site releasing either zero or one vesicle per action potential[15,16] and that release probability on the second stimulus is independent of whether release occurred on the first. For most synapses, r_{1+2}/r_1 fell close to the value predicted for linear summation and well above the line of saturation ($r_{1+2}/r_1 = 1$) (Fig. 4a). Thus, NMDA-R-mediated $[Ca^{2+}]$ responses sum close to linearly, with the second response of a pair producing 0.8 ± 0.08 times the first response (Fig. 4b), translating into a fractional occupancy of less than 0.56 for a single vesicle.

There are several uncertainties in this calculation. First, we may underestimate the amplitude of larger responses because Ca^{2+} indicators have sublinear sensitivity to larger Ca^{2+} changes. Second, we may overestimate the expected number of double releases because the probability of release may be temporarily depressed following a successful release[16,17]. Both these factors bias the calculation towards saturation. On the other hand, glutamate from more than one vesicle (released either by one presynaptic bouton or by several neighbouring boutons) may interact with the same population of NMDA-Rs (multi-vesicular release[18]). In this case, the quantal content due to the second action potential would be greater than assumed, biasing the calculation against saturation. Finally, although CA1 spines receive a single presynaptic contact[8,9], it is possible that some synapses could activate two independent populations of receptors. We consider this unlikely, as it would require perforated synapses with multivesicular release and very effective mechanisms to prevent glutamate diffusion between adjacent receptor populations.

We have shown that synaptic $[Ca^{2+}]$ transients in individual dendritic spines can be used to detect quantal release of neurotransmitter and quantify postsynaptic receptor opening. In contrast to purely electrical recordings, the number and identity of active synapses can be monitored functionally on a trial-by-trial basis. The signal-to-noise ratio of optically detected Ca^{2+} influx mediated by NMDA-Rs exceeds that of electrically detected NMDA-R currents and approaches that of electrically recorded AMPA-R currents. Control experiments demonstrated isolation of NMDA-R-mediated Ca^{2+} influx in our studies. Because the conditions of the intracellular environment were deliberately non-physiological (for example, high dye concentration, prolonged whole-cell washout and depolarization), we do not rule out a physiological role for other Ca^{2+} sources.

NMDA-R-mediated spine $[Ca^{2+}]$ transients are not fully activated by the glutamate released by a single action potential. Rather, a second action potential occurring a short time (10 ms) later causes an additional increase in $[Ca^{2+}]$ at the same spine, implying an underlying increase in NMDA-R opening. The simplest interpretation of our findings is that synaptic NMDA-Rs are not saturated by

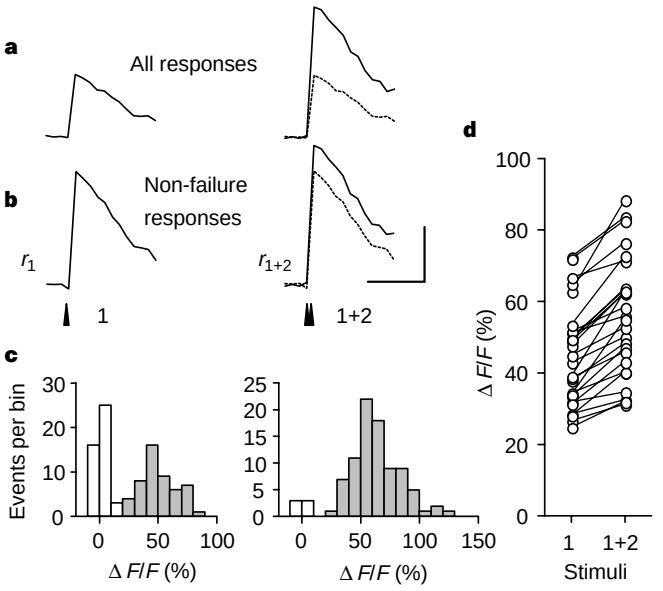

Figure 3 NMDA receptors are not saturated following a single action potential. **a**–**c**, Responses ($\Delta F/F(t)$) for one (left) and two (right) stimuli (10 ms interstimulus interval) at a single spine. **a**, Average of all responses including failures (failure rates: 0.46 and 0.07, respectively). **b**, Average of all responses excluding failures. At this spine, responses to double stimuli were significantly greater than to single stimuli ($r_1 = 50.3 \pm 2.29$ vs $r_{1+2} = 64.0 \pm 2.17\%\ \Delta F/F$, $n = 50, 86$). **c**, Histograms showing the distributions of failure (white bars) and non-failure (shaded bars) response amplitudes. Note shift in distribution to larger amplitudes with double stimuli. Scale bars: 500 ms, 25% $\Delta F/F$. **d**, Average response amplitudes, excluding failures, for all spines tested ($n = 27$). For each spine, the corresponding average single and double stimulus response amplitudes are connected.

glutamate from a single vesicle. This finding is surprising because NMDA-Rs have a high affinity for glutamate and are thought to be outnumbered by a factor of 10–100 by transmitter molecules contained in one vesicle[2]. Studies using kinetic analysis of competitive NMDA-R antagonists[6] and biophysical modelling[19,20] indicated that NMDA-R occupancy could approach 100% after a single action potential (but see ref. 21). Our data indicate that the concentration profile of glutamate reaching NMDA-Rs could be lower or briefer than conventional estimates. The higher temperature in our experiments may allow more effective glutamate clearance, possibly explaining differences between our study and previous ones[6,18]. It could also be that some receptors directly opposite the release site are saturated while other receptors located on the same spine but further from the release site are not.

The absence of saturation of NMDA-Rs has a number of implications for our understanding of the function of excitatory synapses. Lack of saturation implies that the size of NMDA-R responses is limited by the transient concentration of glutamate, rather than the number of functional receptors. Changes in vesicular release or uptake mechanisms may therefore contribute to determining the amplitude and variability of postsynaptic responses. With uptake sufficiently efficient to prevent saturation, crosstalk or spillover between neighbouring synapses[23] would be less prominent than postulated in models assuming saturation[20]. Indeed, even the closest neighbouring spines monitored in our study (~1 μm apart) acted independently, with no evidence of crosstalk (Fig. A of Supplementary Information). If AMPA-Rs are co-localized with NMDA-Rs, they are also likely not to be saturated under similar conditions[18,24,25].

Activation of NMDA-Rs and consequent Ca^{2+} entry into postsynaptic spines are critical to the plasticity of synaptic transmission at many central neurons[26]. The degree of NMDA-R activation can determine whether a synapse undergoes long-term depression or potentiation[27], and the amount of NMDA-R opening depends on membrane potential[28] and hence postsynaptic activity. We have shown that NMDA-R opening is also sensitive to the number of presynaptic quanta released in a short time period. Thus, bursts of presynaptic action potentials may favour induction of potentiation not only by enhancing transmitter release and generally increasing postsynaptic depolarization, but also by enhancing fractional NMDA-R opening and thereby increasing $[Ca^{2+}]$ transients at specific spines. Without saturation, changes in the concentration or rate of clearance of glutamate from the synaptic cleft might also alter the fractional activation of NMDA-Rs by single action potentials and hence modulate plasticity. □

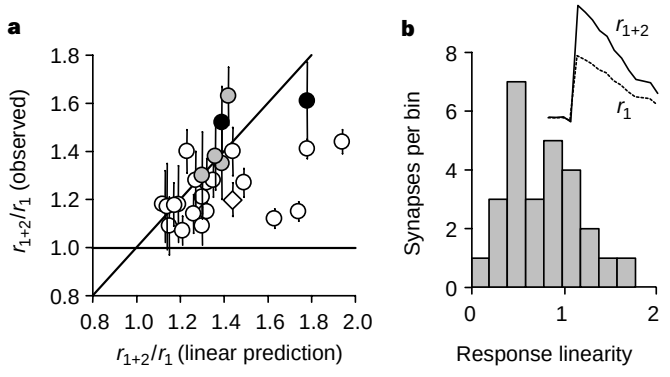

Figure 4 Quantification of NMDA-R response linearity (see Methods for calculation). **a**, Ratios of single to double stimulus non-failure responses, r_{1+2}/r_1, plotted against the predicted ratios assuming linear response summation for each synapse tested. Most synapses are well above saturation (horizontal dashed line). Symbols designate indicator and imaging mode: OGB-1 frame mode (open circles); OGB-2 frame mode (filled circles); OGB-1 line scan mode (grey circles). The diamond corresponds to the synapse represented in Fig. 3a. **b**, NMDA-R response linearity, Δr_{11}. Linearity (absence of saturation) corresponds to a value of $\Delta r_{11} = 1$; saturation corresponds to $\Delta r_{11} = 0$. Inset, comparison of the average relative amplitudes of single (r_1) and calculated double releases ($r_{1+2} = 1.80 r_1$).

Methods

Preparation and electrophysiology. Rat (postnatal day 16–19) hippocampal slices (300–400 μm) were prepared in accordance with the animal care and use guidelines of CSHL. Slices were prepared using a chilled (2–5 °C) cutting solution containing (in mM) 110 choline-chloride, 25 $NaHCO_3$, 25 D-glucose, 11.6 sodium ascorbate, 7 $MgSO_4$, 3.1 sodium pyruvate, 2.5 KCl, 1.25 NaH_2PO_4 and 0.5 $CaCl_2$, and then incubated in physiological saline (127 NaCl, 25 $NaHCO_3$, 25 D-glucose, 2.5 KCl, 2 $CaCl_2$, 1 $MgSO_4$, 1.25 NaH_2PO_4, 0.1 picrotoxin) for 30–60 min at 35 °C and then at room temperature until required. NBQX (5–10 μM) was present in about half of the experiments (otherwise a cut was made between CA3 and CA1). Experiments were done at 35 °C. Whole-cell patch electrodes (2–4 MΩ) contained 135 caesium methylsulphonate, 10 HEPES, 10 sodium phosphocreatine, 4 $MgCl_2$, 4 Na ATP, 0.4 Na-GTP, and 0.2–0.4 Oregon Green BAPTA-1 or 2 (OGB-1, 2). Transmission was evoked by 0.1-ms voltage pulses delivered extracellularly by a glass pipette (2–3 μm tip)[10]. The stimulus intensity was adjusted to minimize failure rate at a target synapse. Control experiments with NBQX, D-CPP and CPA used the same alternating single/double pulse protocol as that used for testing NMDA-R saturation.

Two-photon imaging. We used a custom 2PLSM microscope[10] (software: Lucent Technologies) to image fluorescence transients in CA1 spines. During imaging, the focus was periodically adjusted to correct for drift. Only synapses in which stable responses (determined by plots of $\Delta F/F$) from well-isolated Ca^{2+} sources could be verified (Fig. A of Supplementary Information) were analysed. Relative fluorescence changes were computed as $\Delta F/F(t) = (F(t) - F_0)/F_0$, where F_t is the fluorescence at time t. Baseline fluorescence (F_0) was determined by averaging the four frames (or 240 ms in the line scan) preceding the stimulus. Because background fluorescence was dominated by exogenous dye, it was not subtracted. We averaged the first two frames (50–100 ms in line scan) following the stimulus to calculate the amplitude. The relatively slow timescale over which spine $[Ca^{2+}]$ gradients dissipate[29] facilitated isolation of signals from neighbouring spines (Fig. A of Supplementary Information). The number of trials used to estimate response amplitudes and release probabilities was (median) 77 in frame mode ($n = 26$) and 26 in line-scan mode ($n = 4$). We assume that the influx of Ca^{2+} ions into a spine is proportional to the fraction of doubly bound receptors. To maximize signal-to-noise and avoid possible nonlinearities due to saturation of endogenous Ca^{2+} buffers, we used indicator concentrations large enough to dominate Ca^{2+} binding[30]. To test CPA efficacy on action potential $[Ca^{2+}]$ transients, a low dye concentration (40 μM OGB-1) was used so that the decay was dominated by extrusion and uptake rather than indicator unbinding.

Analysis. We classified transmission failures and successes by eye using the fluorescence response waveform and the corresponding image. The average response evoked by a stimulus pair is $\Sigma p_{ij} r_{ij}$, where i, j indicate failure (=0) or success (=1) of the first (i) or second (j) stimulus, and p_{ij} and r_{ij} are the probabilities and average amplitudes for a given outcome. To calculate response linearity and occupancy, we assume a single release site[8,9] releasing 0 or 1 vesicles per action potential[15,16]; thus $r_1 = r_{01} = r_{10}$, where r_1 is the average non-failure response amplitude for a single stimulus. We define a metric of response linearity, $\Delta r_{11} = (r_{11} - r_1)/r_1$, the fractional amplitude of a response conditioned by a preceding release. $\Delta r_{11} \simeq 0$ implies highly sublinear summation and therefore a high fractional occupancy of receptors after the first release. $\Delta r_{11} \simeq 1$ implies linear summation and therefore low fractional receptor occupancy after the first release. Δr_{11} can be calculated from the non-failure responses to single stimuli (r_1) and to pairs of stimuli (r_{1+2}); according to the definition above, $r_{1+2} = (p_{10} r_1 + p_{01} r_1 + p_{11} r_{11})/(1 - p_{00})$. We further assume that the result of the first stimulus has no effect on the probability of release of the second stimulus. The apparent paired-pulse facilitation is then $PPF = (1 - p_{00}/p_0)/(1 - p_0)$, where p_0 and p_{00} are the measured failure rates for single and double stimuli, respectively. The ratio r_{1+2}/r_1 expected for the saturating (sat, where $r_{11} = r_1$) and linear (lin, where $r_{11} = 2r_1$) cases, in

terms of p_0 and p_{00}, is: $(r_{1+2}/r_1)^{lin} = (2 - p_0 - p_{00}/p_0)/(1 - p_{00})$ and $(r_{1+2}/r_1)^{sat} = 1$. Using the same model, we calculate $\Delta r_{11} = [r_{1+2}(1 - p_{00}) - r_1(1 - p_0)]/(1 - p_0 - p_{00}/p_0 + p_{00})$. As receptor occupancy following the second stimulus is ≤ 1, we can estimate receptor occupancy following the first stimulus to be $\leq 1/(1 + \Delta r_{11})$. The calculation of receptor occupancy does not depend on the origin of release failures and is therefore insensitive to possible unreliability of axonal stimulation. All measurements are given as mean ± s.e.m. unless otherwise noted. The error bars for the observed ratio r_{1+2}/r_1 (Fig. 4a) were calculated by s.e.m. $= \sqrt{s_1^2 + s_{1+2}^2}$, $s_i = \mu_i/(\sigma_i\sqrt{n_i - 1})$, where μ_i, σ_i and n_i are, respectively, the mean, s.d. and number of observations of single and double responses.

Received 23 December 1998; accepted 3 March 1999.

1. Denk, W. & Svoboda, K. Photon upmanship: why multiphoton imaging is more than a gimmick. *Neuron* **18,** 351–357 (1997).
2. Frerking, M. & Wilson, M. Saturation of postsynaptic receptors at central synapses? *Curr. Opin. Neurobiol.* **6,** 395–403 (1996).
3. Tang, C. M., Margulis, M., Shi, Q. Y. & Fielding, A. Saturation of postsynaptic glutamate receptors after quantal release of transmitter. *Neuron* **13,** 1385–1393 (1994).
4. Auger, C., Kondo, S. & Marty, A. Multivesicular release at single functional synaptic sites in cerebellar stellate and basket cells. *J. Neurosci.* **18,** 4532–4547 (1998).
5. Lester, R. A., Clements, J. D., Westbrook, G. L. & Jahr, C. E. Channel kinetics determine the time course of NMDA receptor-mediated synaptic currents. *Nature* **346,** 565–567 (1990).
6. Clements, J. D., Lester, R. A., Tong, G., Jahr, C. E. & Westbrook, G. L. The time course of glutamate in the synaptic cleft. *Science* **258,** 1498–1501 (1992).
7. Yuste, R. & Denk, W. Dendritic spines as basic functional units of neuronal integration. *Nature* **375,** 682–684 (1995).
8. Harris, K. M. & Stevens, J. K. Dendritic spines of CA1 pyramidal cells in the rat hippocampus: Serial electron microscopy with reference to their biophysical characteristics. *J. Neurosci.* **9,** 2982–2997 (1989).
9. Schikorski, T. & Stevens, C. F. Quantitative ultrastructural analysis of hippocampal excitatory synapses. *J. Neurosci.* **17,** 5858–5867 (1997).
10. Mainen, Z. F. *et al*. Two-photon imaging in living brain slices. *Methods: A Companion to Methods in Enzymology* **18** (in the press).
11. Regehr, W. G. & Atluri, P. P. Calcium transients in cerebellar granule cell presynaptic terminals. *Biophys. J.* **68,** 2156–2170 (1995).
12. Markram, H., Helm, P. J. & Sakmann, B. Dendritic calcium transients evoked by single back-propagating action potentials in rat neocortical pyramidal neurons. *J. Physiol. (Lond.)* **485,** 1–20 (1995).
13. Manabe, T. & Nicoll, R. A. Long-term potentiation: evidence against an increase in transmitter release probability in the CA1 region of the hippocampus. *Science* **265,** 1888–1892 (1994).
14. Mainen, Z. F., Jia, Z. P., Roder, J. & Malinow, R. Use-dependent AMPA receptor block in mice lacking GluR2 suggests postsynaptic site for LTP expression. *Nature Neurosci.* **1,** 579–586 (1998).
15. Korn, H., Mallet, A., Triller, A. & Faber, D. S. Transmission at a central inhibitory synapse. II. Quantal description of release, with a physical correlate for binomial n. *J. Neurophysiol.* **48,** 679–707 (1982).
16. Stevens, C. F. & Wang, Y. Facilitation and depression at single central synapses. *Neuron* **14,** 795–802 (1995).
17. Dobrunz, L. E., Huang, E. P. & Stevens, C. F. Very short-term plasticity in hippocampal synapses. *Proc. Natl Acad. Sci. USA* **94,** 14843–14847 (1997).
18. Tong, G. & Jahr, C. E. Multivesicular release from excitatory synapses of cultured hippocampal neurons. *Neuron* **12,** 51–59 (1994).
19. Clements, J. D. Transmitter timecourse in the synaptic cleft: its role in central synaptic function. *Trends Neurosci.* **19,** 163–171 (1996).
20. Rusakov, D. A. & Kullmann, D. M. Extrasynaptic glutamate diffusion in the hippocampus: ultrastructural constraints, uptake, and receptor activation. *J. Neurosci.* **18,** 3158–3170 (1998).
21. Holmes, W. R. Modeling the effect of glutamate diffusion and uptake on NMDA and non-NMDA receptor saturation. *Biophys. J.* **69,** 1734–1747 (1995).
22. Tong, G. & Jahr, C. E. Block of glutamate transporters potentiates postsynaptic excitation. *Neuron* **13,** 1195–1203 (1994).
23. Barbour, B. & Hausser, M. Intersynaptic diffusion of neurotransmitter. *Trends Neurosci.* **20,** 377–384 (1997).
24. Faber, D. S., Young, W. S., Legendre, P. & Korn, H. Intrinsic quantal variability due to stochastic properties of receptor–transmitter interactions. *Science* **258,** 1494–1498 (1992).
25. Silver, R. A., Cull-Candy, S. G. & Takahashi, T. Non-NMDA glutamate receptor occupancy and open probability at a rat cerebellar synapse with single and multiple release sites. *J. Physiol. (Lond.)* **494,** 231–250 (1996).
26. Bliss, T. V. P. & Collingridge, G. L. A synaptic model of memory: Long-term potentiation in the hippocampus. *Nature* **361,** 31–39 (1993).
27. Cummings, J. A., Mulkey, R. M., Nicoll, R. A. & Malenka, R. C. Ca^{2+} signaling requirements for long-term depression in the hippocampus. *Neuron* **16,** 825–833 (1996).
28. Nowak, L., Bregestovski, P., Ascher, P., Herbet, A. & Prochiantz, A. Magnesium gates glutamate-activated channels in mouse central neurons. *Nature* **307,** 462–465 (1984).
29. Svoboda, K., Tank, D. W. & Denk, W. Direct measurement of coupling between dendritic spines and shafts. *Science* **272,** 716–719 (1996).
30. Helmchen, F., Imoto, K. & Sakmann, B. Ca^{2+} buffering and action potential-evoked Ca^{2+} signaling in dendrites of pyramidal neurons. *Biophys. J.* **70,** 1069–1081 (1996).

Supplementary information is available on *Nature*'s World-Wide Web site (http://www.nature.com) or as paper copy from the London editorial office of *Nature*.

Acknowledgements. This work was supported by a Burroughs Wellcome Career Award (Z.F.M.), grants from NIH and the Mather's Foundation (R.M.), and grants from the Pew and Whitaker Foundations (K.S.).

Correspondence and requests for materials should be addressed to K.S. (e-mail: svoboda@cshl.org). A movie of spine Ca^{2+} transients is available on the authors' website (http://www.cshl.org/public/SCIENCE/spine.gif).

Ca^{2+}/calmodulin binds to and modulates P/Q-type calcium channels

Amy Lee, Scott T. Wong, Daniel Gallagher, Bin Li, Daniel R. Storm, Todd Scheuer & William A. Catterall

Department of Pharmacology, University of Washington, Seattle, Washington 98195-7280, USA

Neurotransmitter release at many central synapses is initiated by an influx of calcium ions through P/Q-type calcium channels[1,2], which are densely localized in nerve terminals[3]. Because neurotransmitter release is proportional to the fourth power of calcium concentration[4,5], regulation of its entry can profoundly influence neurotransmission. N- and P/Q-type calcium channels are inhibited by G proteins[6,7], and recent evidence indicates feedback regulation of P/Q-type channels by calcium[8]. Although calcium-dependent inactivation of L-type channels is well documented[9–11],

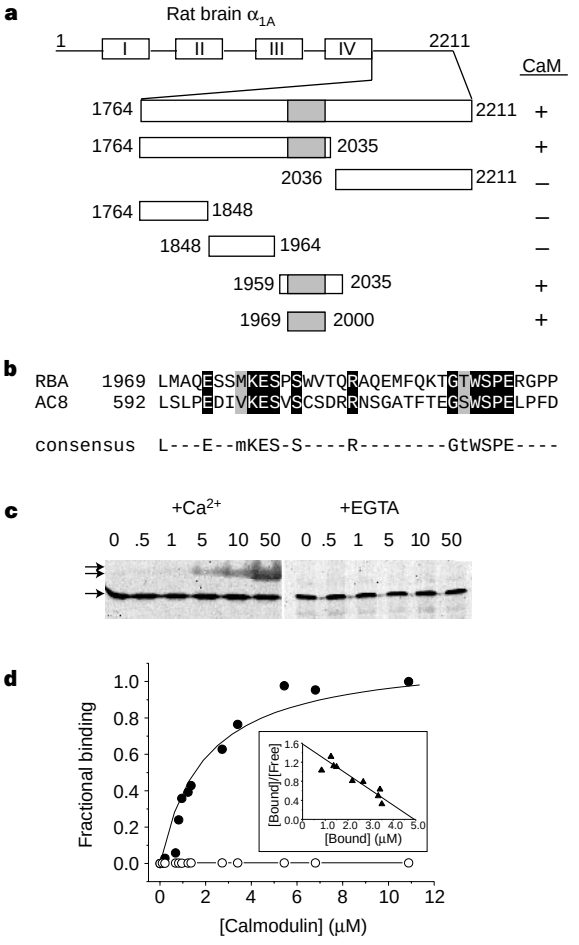

Figure 1 Calmodulin binding to the C-terminal domain of the α_{1A} subunit. **a**, Identification of a calmodulin-binding domain (α_{1A} CBD, shaded region) in α_{1A}. Constructs delimited by the indicated amino acids that interacted with calmodulin (CaM) in the yeast two-hybrid assay are indicated (+). **b**, Alignment of the α_{1A}CBD (RBA) with type 8 adenylyl cyclase (AC8). **c**, Ca^{2+}-dependent binding of α_{1A} CBD peptide (amino acids 1969–2000) to calmodulin in gel-shift assays with the indicated peptide:calmodulin molar ratios. Single arrow, unbound calmodulin; double arrows, peptide-bound calmodulin. **e**, Affinity of α_{1A} CBD for calmodulin estimated by fluorescence anisotropy ($K_d = 1.95 \pm 0.53$ μM). Closed circles, α_{1A} CBD peptide; open circles, control peptide. Inset, Scatchard plot.